

# Nonlinear surface magneto-plasmonics in Kretschmann multilayers

Ilya Razdolski\*, Andrei Kirilyuk, Theo Rasing

*Institute for Molecules and Materials, Radboud University Nijmegen, 6525 AJ Nijmegen, Netherlands*

Denys Makarov, Oliver G. Schmidt

*Institute for Integrative Nanosciences, IFW Dresden, 01069 Dresden, Germany*

Vasily V. Temnov

*Institut des Molécules et Matériaux du Mans, UMR CNRS 6283,*

*Université du Maine, 72085 Le Mans cedex, France*

(Dated: June 26, 2018)

The nonlinear magneto-plasmonics [1–3] aims to utilize plasmonic excitations to control the mechanisms and tailor the efficiencies of the non-linear light frequency conversion at the nanoscale. We investigate the mechanisms of magnetic second harmonic generation in hybrid gold-cobalt-silver multilayer structures, which support propagating surface plasmon polaritons at both fundamental and second harmonic frequencies. Using magneto-optical spectroscopy in Kretschmann geometry, we show that the huge magneto-optical modulation of the second harmonic intensity is dominated by the excitation of surface plasmon polaritons at the second harmonic frequency, as shown by tuning the optical wavelength over the spectral region of strong plasmonic dispersion. Our proof-of-principle experiment highlights bright prospects of nonlinear magneto-plasmonics and contributes to the general understanding of the nonlinear optics of magnetic surfaces and interfaces.

Rapid development of plasmonics has facilitated an outstanding progress in understanding, designing and controlling the optical response of metallic nanostructures, including that in nonlinear-optical domain [4–7]. The optical second harmonic generation (SHG) from solid interfaces represents a well-known experimental technique with numerous applications in physics, chemistry and biology. Being a natural tool to enhance the light-matter interaction, the plasmon-assisted localization of the electric field in small volumes proved to be very effective at elevating the efficiency of the nonlinear-optical processes. Beyond the physics of plasmonic nanoantennas requiring the fabrication of sophisticated metallic nanoobjects [8, 9], the Kretschmann geometry for the excitation of surface plasmon polaritons (SPPs) in a thin metallic layer on a dielectric prism plays a special role due to its robustness and simplicity [10]. A huge plasmonic enhancement of the electric field caused by the phase-matched excitation of SPPs under the resonant coupling conditions has been shown to boost the SHG intensity [11–13]. The most recent experiments have evidenced that not only the SPP-resonance at a fundamental frequency  $\omega$  but also the excitation of a second harmonic SPP at the doubled frequency  $2\omega$  plays an important role in the process of the nonlinear-optical conversion [13, 14]. However, due to their dispersive nature a simultaneous excitation and coupling between the SPPs at fundamental and second harmonic frequencies has not been reported so far.

The main idea of this study was to design a nanoscale optical experiment where we could excite, detect and manipulate the nonlinear interactions between the SPPs at the fundamental and SHG frequencies. To achieve this goal we have adopted the concepts of linear magneto-plasmonics in hybrid metal-ferromagnet multilayer structures [6, 15] together with the most recent ideas in nonlinear magneto-plasmonics [1–3, 16, 17]. Our experimental geometry is sketched in Fig. 1a. A thin gold/cobalt/silver trilayer structure was grown on a glass substrate by means of the magnetron sputtering. A 5 nm-thin magneto-optically active layer of ferromagnetic cobalt was protected from oxidation by a 3 nm-thin layer of gold. A 25 nm-thick silver layer acted as main constituent in this hybrid plasmonic nanostructure, which was excited by collimated femtosecond laser pulses through the glass prism (Kretschmann geometry). The reflected SHG intensity, as well as the linear reflectivity signal at both fundamental  $\omega$  and double frequency  $2\omega$  was recorded as a function of the incidence angle  $\theta$  for the two opposite in-plane directions of magnetization ( $+M$  and  $-M$  in Fig. 1a) of cobalt in the transverse Kerr geometry.

Understanding the properties of the SPP dispersion [18] in our structure (see Fig. 1b and Supplementary Information for details) is one of the key points for nonlinear magneto-plasmonics. Due to inevitable dispersion, the SPP excitations at fundamental and double frequencies in Kretschmann geometry occur at slightly different angles, suggesting that simultaneous phase-matched excitation of both SPPs is impossible. However, nonlinear-optical considerations account

---

\* Present address: Fritz-Haber-Institut der MPG, Phys. Chemie, Faradayweg 4-6, 14195 Berlin, Germany

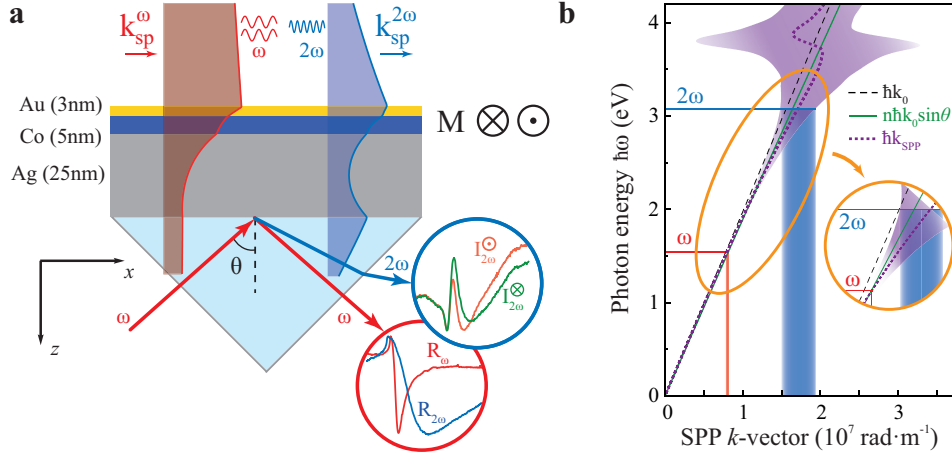


FIG. 1: **Surface plasmons in Au/Co/Ag multilayer structures.** **a** Sketch of the experimental geometry showing the spatial distribution of the square of the normal projection of the electric field at the angles of incidence  $\theta$  corresponding to the SPP excitations at the fundamental  $\omega$  and double  $2\omega$  frequencies. Insets in the coloured circles show the experimental angular dependencies of the linear-optical reflectivity and SHG intensities for the two opposite directions of magnetisation of the cobalt layer. **b** Dispersion of the SPP in the Au/Co/Ag trilayer under study. Black dash and green solid lines represent the photons in vacuum and in glass, respectively. Thick dot purple line is the calculated SPP dispersion, its linewidth is shown with the purple background area. The inset illustrates the possibility of a simultaneous excitation of the SPPs at both frequencies  $\omega$  and  $2\omega$ .

for the following nonlinear phase-matching condition

$$2k_0(\omega)n(\omega)\sin\theta_{\text{nl}} = k_{\text{spp}}(2\omega), \quad (1)$$

between the excitation source at the silver-glass interface characterized by the in-plane component of the  $k$ -vector  $k_0^\omega \sin\theta$  and the second harmonic SPP at the gold-air interface with the  $k$ -vector  $k_{\text{spp}}^{2\omega}$ . Being just one of several possible SPP frequency conversion pathways [13, 19], this phase-matching condition plays a crucial role in our interpretation as it determines the resonant SPP-induced enhancement of the nonlinear susceptibility  $\chi^{(2)}$ .

The experimental results are summarized in Fig. 2. The linear optical reflectivity in Kretschmann configuration using the fundamental (920 nm) and second harmonic wavelengths (460 nm, frequency doubled in a BBO-crystal) are displayed in Fig. 2a. A narrow plasmonic reflectivity dip at 920 nm observed at 42.5 degrees contrasts with a much broader minimum at 460 nm at  $\theta \approx 47$  degrees, in agreement with much higher SPP-losses at  $2\omega$ . In terms of linear magneto-plasmonics these two resonances behave similarly: the relative magnetisation-induced variations of the reflectivity,  $\Delta R/R$  neatly follow the angular differential reflectivity  $dR/d\theta$ , suggesting that altering the magnetization direction induces a small shift of the reflectivity spectrum due to the magnetic contribution to the SPP wavevector [4, 20].

Whereas the linear reflectivity at fundamental frequency  $\omega$  shows only small modulations of the order of 1%, in line with Ref. [6], the SHG angular spectra at  $2\omega$  display drastic changes, as shown in Fig. 2b for four different values of the fundamental wavelength 760, 800, 820 and 920 nm. Red and blue background areas show the SPP dispersion (see Fig. 1b) at the frequencies  $\omega$  and  $2\omega$ , respectively, recalculated as a function of incidence angle  $\theta$ . Over the SHG wavelengths range (380-460 nm) the SPP shows a strongly dispersive behavior resulting in a shift of the resonant angle and decrease of losses (see the linewidth). Fundamental SPP remains nearly dispersionless and demonstrates no noticeable change of its linewidth. Contrary to previously reported results on a gold film [14], the angular positions of the SPP resonances for the fundamental and SHG frequencies in our multilayer structure correspond to the pronounced minima in the SHG intensity. A strong dependence of SHG intensity on magnetization direction  $I_{2\omega}(\pm M)$  is quantified by the magnetic SHG (mSHG) contrast  $\rho$ :

$$\rho = \frac{I_{2\omega}(+M) - I_{2\omega}(-M)}{I_{2\omega}(+M) + I_{2\omega}(-M)}, \quad (2)$$

shown in Fig. 2d. Surprisingly, the largest magnetisation-induced modulation of the SHG intensity is accompanied by the SPP excitation at the SHG frequency and not the fundamental one. Angular dependence of mSHG contrast re-plotted in Fig. 2e without an offset displays the largest reported values of modulation reaching 33 % around  $\theta = 44$  degrees. For the shortest wavelength (760 nm) the mSHG maximum is only about 20%, since in this case the

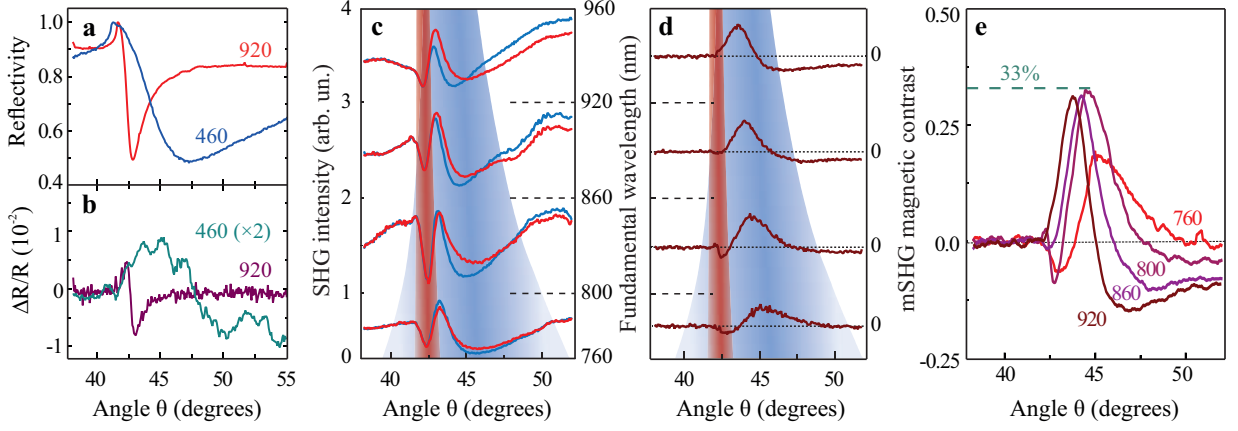


FIG. 2: **Angular spectra of the linear and nonlinear magneto-optical response in presence of the SPPs.** **a,b** Linear-optical reflectivity  $R$  and magnetization-induced reflectivity variations  $\Delta R/R$  for the excitation with the 920 and 460 nm wavelength. **c,d** SHG intensity and (d) mSHG contrast  $\rho$  angular spectra plotted with an offset. Red and blue background areas illustrate the SPP dispersion in the experimental spectral range (760-920 nm for fundamental, 380-460 for the SHG, respectively.) **e** Angular spectra of the mSHG magnetic contrast  $\rho$  for the four fundamental wavelengths, no offset is introduced. Inset: Illustration of the magnetisation-induced changes of the total SHG intensity,  $I_{2\omega}(\pm M) \propto |\vec{E}^{2\omega}(\pm M)|^2 = |\vec{E}^{2\omega} \pm \vec{E}_m^{2\omega}|^2$ .

SPP damping at the SHG frequency becomes so large that the system approaches the region with the non-propagating (propagation length  $\lambda^{\text{SPP}} < \lambda_{2\omega}$ ) SPPs. This observation links up our measurements to the most recent results by Zheng *et al.* [2], who reported similar values of the mSHG contrast on a 10 nm-thin iron film on glass, a structure not supporting SPPs at the SHG frequency. This fact, along with the dispersive shift of mSHG maximum reinforces our conclusion that the 33 % large mSHG contrast (which is equivalent to the increase of the SHG intensity by a factor of 2 upon magnetization reversal) is dominated by the SPP resonance at the SHG frequency.

In order to understand these experimental observations we have used the approach proposed by Palomba and Novotny [14], who explained the complex angular dependence of the SHG intensity from a thin gold film on glass by an interference of two contributions coming from the gold-air and gold-glass interfaces. In our case (Fig. 3a) the silver-sapphire interface acts as a source of the nonmagnetic SHG  $\vec{E}_1^{2\omega}$ , and the upper part consisting of Au and Co layers is assumed to generate the electric field  $\vec{E}_2^{2\omega}$  containing both magnetic  $\chi^{(2m)}$  and non-magnetic  $\chi^{(2)}$  contributions. Thus the total SHG intensity  $I_{2\omega}$  is described by:

$$I_{2\omega} \propto |\vec{E}_1^{2\omega} + \vec{E}_2^{2\omega} \pm \vec{E}_{2m}^{2\omega}| = |\chi_1^{(2)} : \vec{E}_1 \vec{E}_1 + \chi_2^{(2)} : \vec{E}_2 \vec{E}_2 \pm \chi_2^{(2m)} : \vec{E}_2 \vec{E}_2|^2, \quad (3)$$

where complex tensor components  $\chi_1^{(2)}$  and  $\chi_2^{(2)} \pm \chi_2^{(2m)}$  represent the effective optical nonlinearities at both interfaces. The angular dependences of the electric fields  $\vec{E}_1$  and  $\vec{E}_2$  at the fundamental frequency  $\omega$ , which are driving the SHG process at both interfaces, are calculated by finite difference time domain (FDTD) method for the 860 nm excitation wavelength (see Fig. 3c-d).

Based on these calculations, the modulation of SHG intensity in the vicinity of fundamental SPP resonance can be explained by destructive interference of two contributions  $\vec{E}_1^{2\omega}$  and  $\vec{E}_2^{2\omega}$  [14]. For our multilayer structure the amplitude of the SHG light generated at the upper interface and transmitted through the prism at any angle  $\theta$  turns out to be smaller as compared to the other one:  $|\vec{E}_2^{2\omega}| < |\vec{E}_1^{2\omega}|$ . This is why the strong increase of  $\vec{E}_2$  in Fig. 3c-d at the top interface explains the SHG intensity minimum around the fundamental SPP resonance at  $\theta = 42.5$  degrees.

The same explanation holds for the SHG minimum around  $\theta = 45$  degrees albeit for a different reason. We note that the nonlinear susceptibility  $\chi^{(2)}$  is known to acquire a SPP-induced resonant contribution,  $\chi^{(2)} = \chi_{\text{nr}}^{(2)} + \chi_{\text{res}}^{(2)}$  [11, 21] with:

$$\chi_{\text{res}}^{(2)}(\theta) \propto \frac{1}{\theta - \theta_{\text{nl}} + i\Gamma}. \quad (4)$$

Owing to this resonant contribution, the SHG field enhanced at the top interface destructively interferes with the one generated at the bottom interfaces, which explains the experimentally observed SHG intensity minimum. In order to understand the angular spectrum of this resonant contribution we approximated it with the Lorentzian resonance line. The width  $\Gamma$  and the angular position  $\theta_{\text{nl}}$  of this resonance line was chosen according to the calculations shown in Fig. 1b for the nonlinear SPP excitation at frequency  $2\omega$ , or 430 nm wavelength. This resonant shape successfully

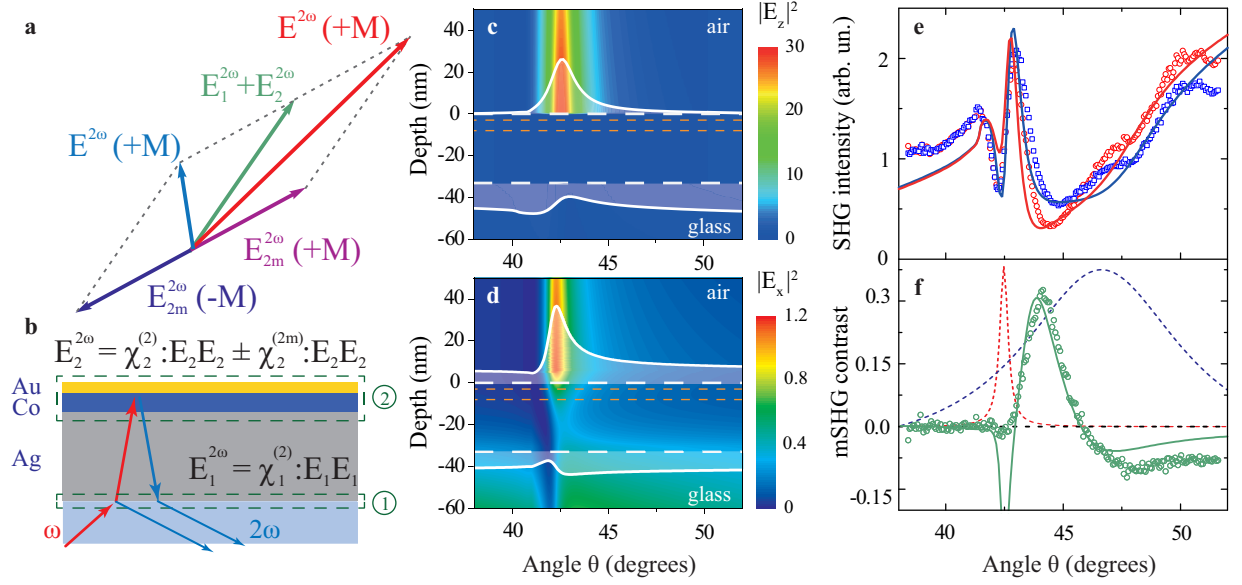


FIG. 3: **Schematics of the SPP-assisted mSHG generation in a multilayer structure.** **a** Illustration of the origin of the inequality of the SHG intensities for the opposite direction of the external magnetic field  $H$  leading to the non-zero magnetic contrast  $\rho$ . **b** SHG sources at the two interfaces, bottom (1, glass/Ag) and top (2, air/Au/Co/Si). **c-d** False colour spatial distributions of the square of the electric field projections  $|E_z|^2$  and  $|E_x|^2$  at the 860 nm fundamental wavelength. Dashed white lines show the sample borders. Solid white lines represent the corresponding  $|E|^2$  angular distributions at the top and bottom interfaces. **e-f** SHG intensity and mSHG contrast angular spectra (open circles and squares) for the 860 nm fundamental wavelength together with the fit lines based on the Eq. (3). Dashed lines are the angular profiles corresponding to the resonant SPP excitation at the frequency  $\omega$  and nonlinear SPP excitation  $\omega \rightarrow 2\omega$  (see Fig. 5S in the Supplementary Information).

accounts for the large mSHG modulation at the angles corresponding to the nonlinear SPP excitation quantified by Eq. (1). Based on Eq. (3) we were able to fit the experimental angular spectra using the resonant part of the nonlinear susceptibility  $\chi_{\text{res}}^{(2)}$  only.

Leaving out the details of our fitting of Eq. (3) for the Supplementary Information, where the choice of predominant  $\chi^{(2)}$  components (from the six non-zero ones, three magnetic and three non-magnetic, at each interface) also justified, we would like to claim to have obtained a good quantitative agreement between the theory and experiment both for angular dependence of the SHG intensity (Fig. 3e) and mSHG contrast (Fig. 3f). Note that the mismatch between the experimental data and the fit curves occurs largely around the fundamental SPP resonance, where the resonant  $\chi^{(2)}$  contribution used in our simulations is hardly playing any role.

Based on our numerical calculations, we can conclude that the large value (33%) of mSHG contrast is dominated by the properties of SPP resonance at SHG frequency. Thus, upon reversing the external magnetic field the SHG output can be doubled, which opens up a new strategy for the design of nonlinear magneto-phonic devices operating at the nanoscale. The frequency dependence over the dispersive SPP spectral range clearly demonstrated that the maximum value of 33% mSHG contrast remains large whereas its angular width decreases as the SHG resonance gets narrower and shifts towards the fundamental resonance.

In the given spectral range one would expect to reach further enhancement of mSHG contrast by systematically varying the individual thicknesses in this trilayer structure. The future route for investigations will imply moving towards the experiments in the telecom frequency range, which apart from the obvious technological importance would allow to extend the magneto-optical investigations including the magnetization-induced third harmonic generation. Moreover, expanding into the far-IR or THz spectral range, where the SPP dispersion is lower, would allow to explore the phase-matched magneto-plasmonic coupling between the SPPs at the fundamental, second, third and higher-order harmonic frequencies. With the largest reported plasmon-assisted value of mSHG contrast of 33% we get closer to

the dream of the nonlinear magneto-photonic devices based on novel physical principles.

- 
- [1] Razdolski, I. *et al.* Nonlocal nonlinear magneto-optical response of a magnetoplasmonic crystal. *Phys. Rev. B* **88**, 075436 (2013). URL <http://link.aps.org/doi/10.1103/PhysRevB.88.075436>.
- [2] Zheng, W., Hanbicki, A., Jonker, B. T. & Lüpke, G. Control of magnetic contrast with nonlinear magneto-plasmonics. *Sci. Rep.* **4**, 1–5 (2014).
- [3] Krutyanskiy, V.L. *et al.* Giant nonlinear magneto-optical response of magnetoplasmonic crystals. *Phys. Rev. B* **91**, 121411(R) (2015). URL <http://link.aps.org/doi/10.1103/PhysRevB.91.121411>.
- [4] Temnov, V. V. *et al.* Active magneto-plasmonics in hybrid metal-ferromagnet structures. *Nat. Photon.* **4**, 107–111 (2010).
- [5] Kauranen, M. & Zayats, A. V. Nonlinear plasmonics. *Nat. Photon.* **6**, 737–748 (2012).
- [6] Armelles, G., Cebollada, A., García-Martín, A. & González, M. U. Magnetoplasmonics: Combining magnetic and plasmonic functionalities. *Adv. Opt. Mater.* **1**, 10–35 (2013).
- [7] Belotelov, V. I. *et al.* Plasmon-mediated magneto-optical transparency. *Nature Comm.* **4**, 2128 (2013). URL <http://dx.doi.org/10.1038/ncomms3128>.
- [8] Novotny, L. & van Hulst, N. Antennas for light. *Nat. Photon.* **5**, 83–90 (2011).
- [9] Hanke, T. *et al.* Tailoring Spatiotemporal Light Confinement in Single Plasmonic Nanoantennas. *Nano Lett.* **12**(2), 992–996 (2012).
- [10] Kretschmann, E. & Raether, H. Radiative Decay of Non Radiative Surface Plasmons Excited by Light. *Z. Naturforsch.* **23a**, 2135–2136 (1968).
- [11] Simon, H. J., Mitchell, D. E. & Watson, J. G. Optical second-harmonic generation with surface plasmons in silver films. *Phys. Rev. Lett.* **33**, 1531–1534 (1974). URL <http://link.aps.org/doi/10.1103/PhysRevLett.33.1531>.
- [12] Naraoka, R., Okawa, H., Hashimoto, K. & Kajikawa, K. Surface plasmon resonance enhanced second-harmonic generation in kretschmann configuration. *Optics Comm.* **248**, 249 – 256 (2005). URL <http://www.sciencedirect.com/science/article/pii/S0030401804012519>.
- [13] Grosse, N. B., Heckmann, J. & Woggon, U. Nonlinear plasmon-photon interaction resolved by k-space spectroscopy. *Phys. Rev. Lett.* **108**, 136802 (2012).
- [14] Palomba, S. & Novotny, L. Nonlinear excitation of surface plasmon polaritons by four-wave mixing. *Phys. Rev. Lett.* **101**, 056802 (2008). URL <http://link.aps.org/doi/10.1103/PhysRevLett.101.056802>.
- [15] Temnov, V. V. Ultrafast acousto-magneto-plasmonics. *Nat. Photon.* **6**, 728736 (2012).
- [16] Krutyanskiy, V. *et al.* Plasmonic enhancement of nonlinear magneto-optical response in nickel nanorod metamaterials. *Phys. Rev. B* **87**, 035116 (2013).
- [17] Chekhov, A. L. *et al.* Wide tunability of magnetoplasmonic crystals due to excitation of multiple waveguide and plasmon modes. *Opt. Express* **22**, 17762–17768 (2014). URL <http://www.opticsexpress.org/abstract.cfm?URI=oe-22-15-17762>.
- [18] Dionne, J. A., Sweatlock, L. A., Atwater, H. A. & Polman, A. Planar metal plasmon waveguides: frequency-dependent dispersion, propagation, localization, and loss beyond the free electron model. *Phys. Rev. B* **72**, 075405 (2005). URL <http://link.aps.org/doi/10.1103/PhysRevB.72.075405>.
- [19] Heckmann, J., Kleemann, M.-E., Grosse, N. B. & Woggon, U. The dual annihilation of a surface plasmon and a photon by virtue of a three-wave mixing interaction. *Opt. Express* **21**, 28856–28861 (2013). URL <http://www.opticsexpress.org/abstract.cfm?URI=oe-21-23-28856>.
- [20] González-Díaz, J. B. *et al.* Surface-magnetoplasmon nonreciprocity effects in noble-metal/ferromagnetic heterostructures. *Phys. Rev. B* **76**, 153402 (2007). URL <http://link.aps.org/doi/10.1103/PhysRevB.76.153402>.
- [21] Raschke, M., Hayashi, M., Lin, S. & Shen, Y. Doubly-resonant sum-frequency generation spectroscopy for surface studies. *Chem. Phys. Lett.* **359**, 367–372 (2002).
- [22] Heinz, T.F. *Second-order nonlinear optical effects at surfaces and interfaces in Nonlinear Surface Electromagnetic Phenomena*, H.-E. Ponath, and G. I. Stegeman (eds.), Elsevier, Amsterdam (1991).

### Acknowledgements

The authors are indebted to Dr. T.V. Murzina for stimulating discussions and to the Region Pays de La Loire for funding.

### Author contributions

All authors have contributed to this paper and agree to its contents. I.R., V.V.T., and Th.R. wrote the proposal. I.R. and V.V.T. conceived and designed the experiments, performed the measurements and analyzed the data. D.M. and O.G.S. prepared and characterized the samples. A.K, Th.R., D.M., and O.G.S. contributed materials and analysis tools. I.R. and V.V.T. wrote the manuscript. All authors contributed to the discussion of the results.

### Competing interests

The authors declare that they have no competing financial interests.

### Correspondence

Correspondence and requests for materials should be addressed to I.R. (email: razdolski@fhi-berlin.mpg.de) or V.V.T. (email: vasily.temnov@univ-lemans.fr).

### Supplementary information

#### Surface plasmon dispersion in Au/Co/Ag trilayers

In order to obtain the surface plasmon polariton (SPP) dispersion relation [1]

$$k_{\text{spp}}(\omega) = k'_{\text{spp}} + ik''_{\text{spp}} = k_0(n'_{\text{spp}} + in''_{\text{spp}}) = k_0 \sqrt{\frac{\varepsilon_{\text{eff}}}{1 + \varepsilon_{\text{eff}}}}, \quad (5)$$

which is characterized by frequency-dependent SPP wavevector  $k_{\text{spp}}(\omega)$  or refractive index  $n_{\text{spp}} = n'_{\text{spp}} + in''_{\text{spp}}$  we applied the effective medium theory. It allowed us to approximate the effective dielectric constant of the Au/Co/Ag interface [2]:

$$\varepsilon_{\text{eff}} = \frac{1}{\delta_{\text{skin}}} \int_0^{\infty} \varepsilon(z) e^{-z/\delta_{\text{skin}}} dz, \quad (6)$$

where the dielectric function  $\varepsilon(z)$  depends on the normal coordinate  $z$  inside the multilayer structure. The spectral dependence of the dielectric function for gold, cobalt and silver is taken from Ref. [3]. The total thickness of two upper metal layers (3 nm Au and 5 nm Co) is significantly smaller than the penetration depth of the electric field  $\delta_{\text{skin}} \sim 12$  nm.

In order to explain the results of the graphical representation in Fig. 1b we would like to quantitatively compare the SPP dispersion relations at Ag/air and Ag/5nm Co/3nm Au/air interfaces. Figure 1S shows the wavelength dependence of the real ( $n'_{\text{spp}}$ ) and imaginary ( $n''_{\text{spp}}$ ) parts of the SPP refractive index as well as the SPP skin depth and propagation length  $L_{\text{spp}}$ . The presence of a highly absorbing cobalt layer in our multilayer structure leads to a significant reduction of the SPP propagation length  $L_{\text{spp}} = 1/(2k_0 n''_{\text{spp}})$  over the entire spectral range, as compared to the Ag-air interface. In contrast to this behavior, the skin depth  $\delta_{\text{skin}}$  and the real part of SPP refractive index  $n'_{\text{spp}}$  exhibit substantial differences only in the vicinity of the SPP resonance corresponding to an optical wavelength in vacuum of 350 nm. Moreover, in the entire spectral range of our SHG measurements (380-460 nm for SHG and 760-920 nm for fundamental wavelength), the skin depths for both structures appear to be nearly identical. This allows us to calculate  $\varepsilon_{\text{eff}}$  in Eq. (6) using the skin depth for the Ag-air interface.

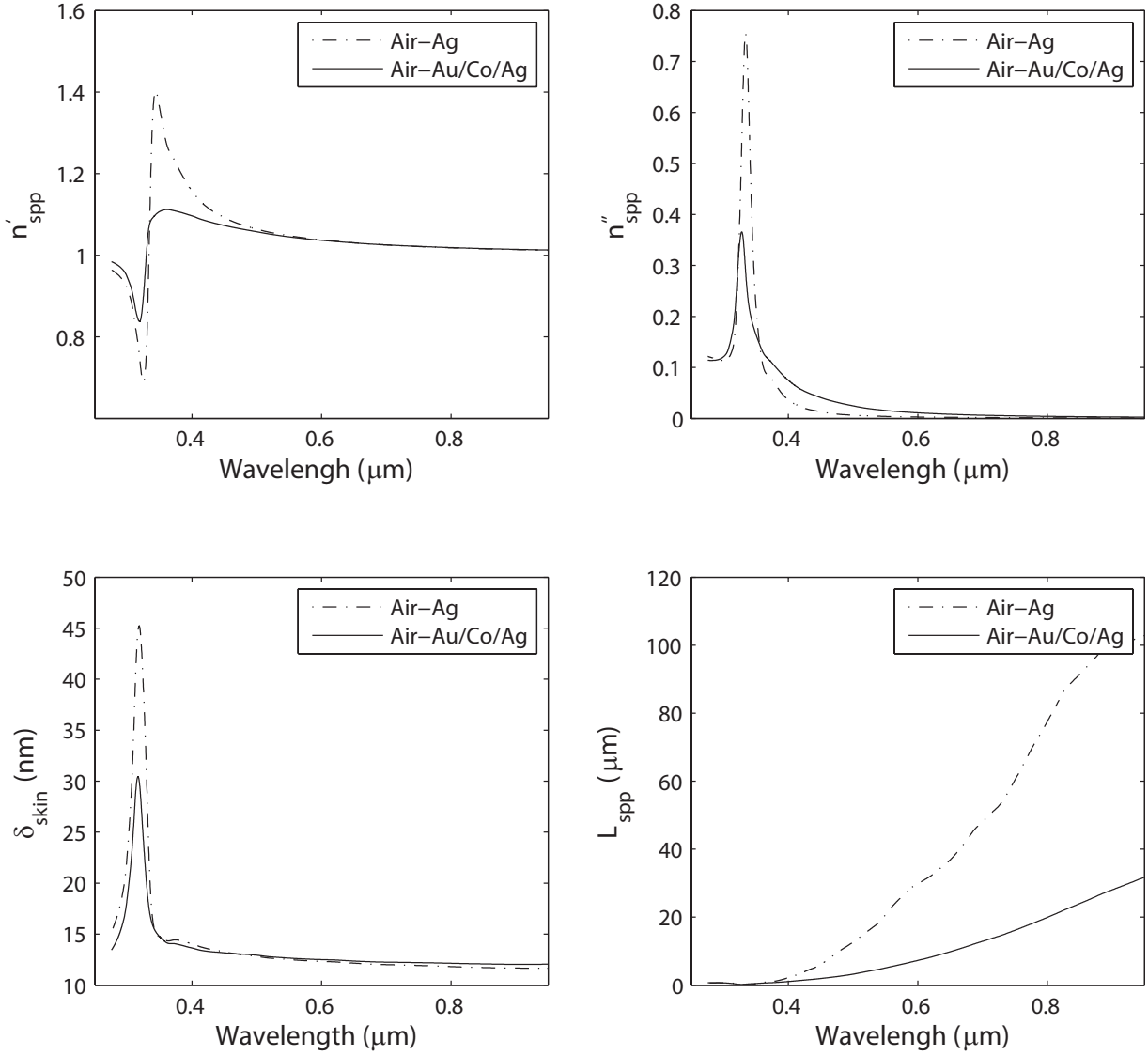


Figure 1S: Spectra dependence of complex refractive index  $n_{\text{spp}} = n'_{\text{spp}} + in''_{\text{spp}}$ , skin depth  $\delta_{\text{skin}}$  and propagation distance  $L_{\text{spp}}$  for the SPPs excited at the air-Ag and air-Au/Co/Ag interfaces.

Now we turn to the discussion of Fig. 1 in the main manuscript. Due to substantial losses the (linear) resonance condition in Kretschmann configuration

$$k_x(\theta, \omega) = k'_{\text{spp}}(\omega) \quad (7)$$

with  $k_x(\theta, \omega) = k_0(\omega)n(\omega)\sin\theta$  appears to be fulfilled within a finite range of incident angles  $\theta$  (or tangential components  $k_x(\theta, \omega)$  of optical wavevectors in the prism).

To account for this angular broadening, we have applied a simple phenomenological model, where the complex Lorentzian-shaped function  $f(k_x, \omega)$  determines the efficiency of the SPP excitation:

$$f(k_x, \omega) = \frac{k''_{\text{spp}}(\omega)}{(k'_{\text{spp}}(\omega) - k_x) + ik''_{\text{spp}}(\omega)}, \quad (8)$$

or, equivalently

$$f(\theta, \omega) = \frac{k''_{\text{spp}}(\omega)}{(k'_{\text{spp}}(\omega) - k_0(\omega)n(\omega)\sin\theta) + ik''_{\text{spp}}(\omega)}. \quad (9)$$

The shaded areas in Fig. 1b and Fig. 2c,d in the main manuscript are limited by two contours of this angular distribution at the half-maximum of this Lorentzian  $|f(k_x, \omega)|^2$  or  $|f(\theta, \omega)|^2$ .

### Linear reflectivity in presence of SPPs

Angular dependence of the linear reflectivity in Kretschmann geometry was measured for eight different wavelengths, namely 760, 800, 860, 920 nm at fundamental laser frequencies and 380, 400, 430 and 460 nm with its second harmonic light (generated in a BBO-crystal before the sample), see Fig. 2S(a,b). Maximum values of the reflectivity are normalized to unity because these supplementary measurements were not calibrated to get absolute values. Angular spectra of the magneto-optical Kerr effect measured at the four fundamental frequencies (Fig. 2S,c) demonstrate great similarity to each other due to low SPP-dispersion in this spectral region.

Despite the fact that the curves measured in the blue ( $2\omega$ ) range also look somewhat similar, the change of the resonant dip when decreasing the wavelength is still noticeable. Figure 2S(c,d) illustrates angular spectra of the transverse Kerr effect at the same wavelengths. Note the characteristic asymmetric shape of the spectra, present for both red and blue sets of wavelengths. It is worth mentioning that the transverse Kerr effect at blue wavelengths is several times smaller than at the red ones, which obviously correlates with the quality factor of the SPP resonance. Furthermore, the magnitude of the magnetoplasmonic modulation of the reflectivity decreases when the wavelength approaches 380 nm. This observation can be explained by comparing the propagation length of a SPP  $L_{\text{spp}}$  with the light wavelength  $\lambda$  (see Fig. 1S). It is seen that  $L_{\text{spp}}$  decreases together with the fundamental wavelength, thus reducing the quality of the SPP excitation and also the Co magnetization-induced contribution to the SPP  $k$ -vector. As the latter is directly responsible for the SPP-assisted magnetoplasmonic reflectivity modulation, the transverse magneto-optical Kerr effect also decreases, albeit a very broad dip in the reflectivity is still seen.

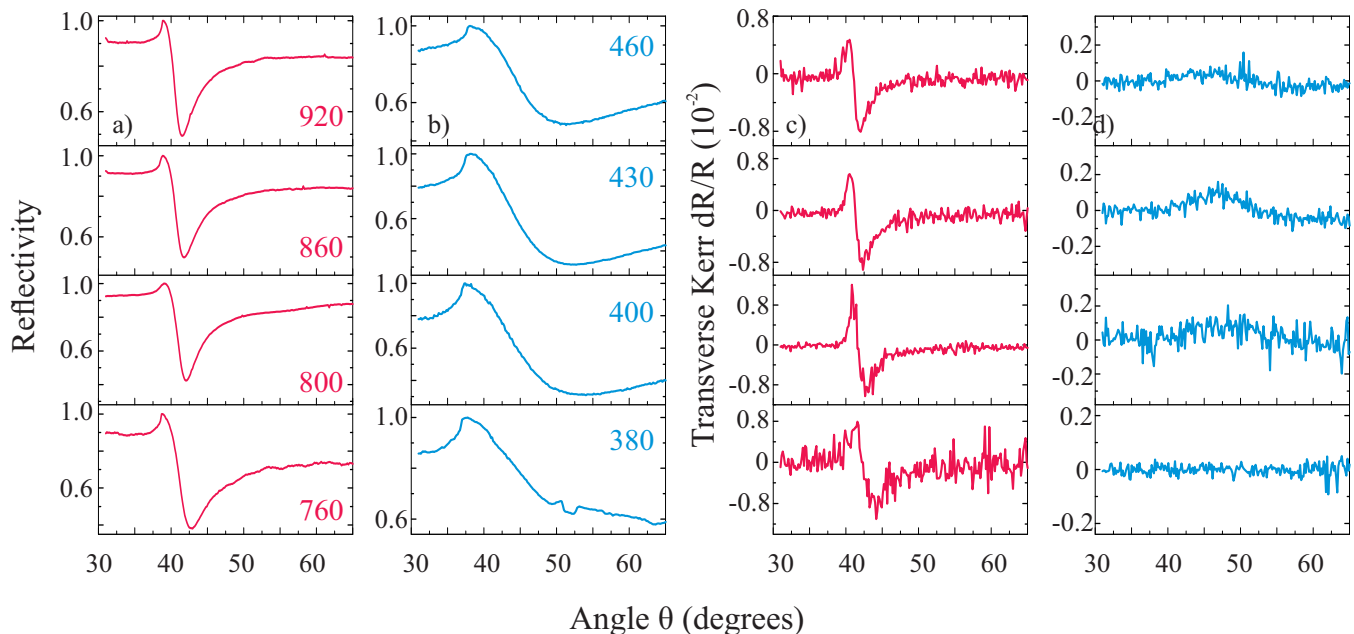


Figure 2S: (a-b) Angular spectra of the SPP-modulated reflectivity  $R$  for the four red (a) and blue (b) wavelengths. (c-d) Angular spectra of the magneto-optical transverse Kerr reflectivity modulation  $dR/R$  for the same wavelengths.

### Nonlinear-optical SPP excitation

A conventional way of exciting a SPP in the linear optics requires the linear phase-matching condition (7) to be fulfilled [1]. This linear phase-matching condition describes an SPP excitation at a frequency  $\omega$ . However, this phase-matching condition appears to be modified, if an SPP is generated via the nonlinear frequency mixing, *i.e.* surface second harmonic generation (SHG) at the frequency  $2\omega$  [4, 5]. A straightforward analogy with SHG generation in a nonlinear crystal directly leads to the following phase-matching condition

$$k_x(\omega) + k_x(\omega) = 2k_0(\omega)n(\omega) \sin \theta = k'_{\text{spp}}(2\omega) \quad (10)$$



for two incident photons generate generate an SPP at doubled frequency. As in case of linear resonance this phase-matching condition is broadened by SPP-dissipation

$$f_{\text{nl}}(k_x, 2\omega) = \frac{k''_{\text{spp}}(2\omega)}{(k'_{\text{spp}}(2\omega) - 2k_x(\omega)) + ik''_{\text{spp}}(2\omega)}. \quad (11)$$

Due to very high plasmonic losses the acceptance angle for phase-matched SPP generation at  $2\omega$  is much larger as compared to the linear phase-matching at the fundamental frequency. Note that this nonlinear phase-matching condition slightly differs from the linear phase-matching condition for a collimated beam at frequency  $2\omega$ :

$$f(k_x, 2\omega) = \frac{k''_{\text{spp}}(2\omega)}{(k'_{\text{spp}}(2\omega) - k_x(2\omega)) + ik''_{\text{spp}}(2\omega)}. \quad (12)$$

Comparing the expressions for  $2k_x(\omega) = 2k_0n(\omega)\sin\theta$  and  $k_x(2\omega) = 2k_0n(2\omega)\sin\theta$  we recognize that the angles for the phase-matched SHG generation and linear excitation in Kretschmann configuration are different only due to dispersion in a glass prism:  $n(\omega) \neq n(2\omega)$ . Knowing this small angular shift of about 0.7 degree between  $f_{\text{nl}}(\theta, 2\omega)$  and  $f(\theta, 2\omega)$  for 860 nm fundamental wavelength, we can correctly calculate the SPP-assisted field enhancement at  $2\omega$  from the linear reflectivity in Kretschmann configuration. As we will see below, this analysis appears to be particularly useful to estimate the angular dependence of the resonant part of the  $\chi^{(2)}$ -tensor.

## Fitting experimental data

### General considerations

Trying to identify the leading tensor contributions in second harmonic generation from a isotropic surface is a delicate issue of playing with three possible contributions (consider p-polarised fundamental and SHG beams):  $\chi_{zzz}^{(2)}$ ,  $\chi_{zxx}^{(2)}$  and  $\chi_{xzx}^{(2)}$  [6]. In the chosen Cartesian coordinate frame  $z$ -axis is perpendicular to the surface plane and  $x$ -axis lies in the incidence plane.

There are multiple considerations regarding the appropriate choice of the nonlinear susceptibility components, if their values are *a priori* not known. The trajectory of free electrons moving in the direction perpendicular to the interface ( $z$ -direction) is expected to exhibit the largest nonlinearities due to the structural changes across the interface (a large built-in electric field at the interface explaining the physical origin of the work function/contact potential) [7]. Therefore the  $\chi_{zzz}^{(2)}$  component is expected to dominate in a free-carrier approximation, when the energy of SHG photon is smaller than the energy separation  $E_g$  between the Fermi level and the  $d$ -band. This is indeed the case for silver, as  $E_g = 3.8$  eV exceeds the largest photon energy used in our experiments (3.3 eV). As described in the main Manuscript, there are two sources of SHG in our model, which are located at the Ag/glass and Ag/Co/Au/air interfaces. Given that all our attempts to get reasonable fits with the components other than  $\chi_{1,zzz}^{(2)}$  at Ag/glass interface failed, we fixed this  $zzz$ -component in further simulations described below. We attribute the ability to identify the dominant tensor component to the aforementioned fact that both relevant frequencies  $\omega$  and  $2\omega$  are below the  $d$ -band edge in silver.

The above conclusions largely rely on the ongoing debates regarding the choice of the most important components of the nonlinear susceptibility  $\chi^{(2)}$  [7–13]. Naraoka *et al.* [10] demonstrated that  $\chi_{zzz}$  yields a better agreement with the experimentally observed SHG output enhancement. The same conclusion is implicitly confirmed by other authors [7, 11]. However, several authors [12, 13] consider instead the  $\chi_{xzx}$  component, following the original paper by Simon *et al.* [14], which nonetheless claims the similar behaviour of all three components in the vicinity of the SPP resonance. Note the rigorous, although somewhat less instructive approach used by Pavlov *et al.* [15], where all components were taken into account, and thus the number of the fit parameters increased dramatically. We attribute these discrepancies to a simple observation that it is generally difficult to isolate the dominant contribution to  $\chi^{(2)}$  tensor if either the fundamental or SHG-frequencies overlap with interband transitions.

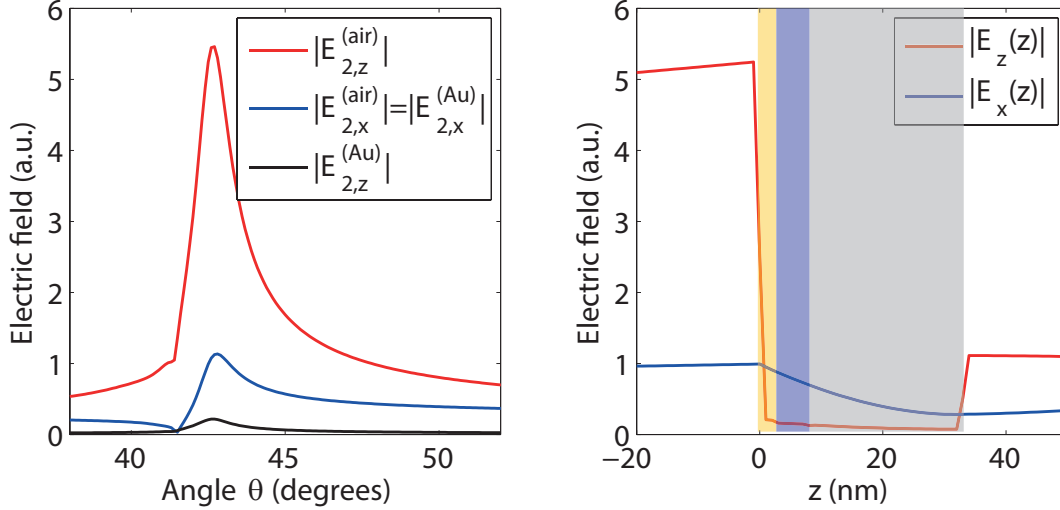


Figure 3S: (a) Angular dependence of electric fields at the gold-air interface. Whereas the tangential component  $E_x$  is continuous across the interface, the normal component  $E_z$  experiences a large jump. (b) Dependence of electric field on the normal coordinate  $z$  at  $\theta = 42.5^\circ$  corresponding to the SPP excitation at the frequency  $\omega$ .

However, different contributions  $P_i^{2\omega} = \chi_{ijk}^{(2)} E_j E_k$  to the non-linear polarization also depend on the components of the local electric field  $E_{j,k}$ . The boundary conditions in Maxwell equations dictate the continuity of the tangential component of the electric field  $E_x$  and the normal component of displacement field  $D_z = \varepsilon(z)E_z$  across the interfaces. In our plasmonic case characterized by  $|\varepsilon_{Au}| \gg 1$  the boundary conditions suggest  $E_z \gg E_x$  in the dielectrics (air and glass) and  $E_z \ll E_x$  in Ag, Au and Co. This statement is confirmed by Finite Difference Time Domain calculations of the electric fields for our structure leading to  $|E_x|^2 \simeq 25|E_z|^2$  for electric fields *inside* the metal and thus explaining why we have obtained better fits considering the  $\chi_{ixx}^{(2)} E_x^2$  contributions. We would like to note for the sake of completeness that on the air side the relation is opposite:  $|E_x|^2 \simeq 0.04 |E_z|^2$ . This suggests that the nonlinear-optical response of our plasmonic structures covered with a nonlinear medium (such as, for example, a monolayer of molecules or semiconductor quantum dots) will be probably dominated by different contributions to the optical nonlinearity.

#### Fitting SHG intensity

As a first step in the fitting procedure we decided to try different  $\chi^{(2)}$  components at the top interface, in attempt to figure out which one is the most important for the observed modulations of the SHG-signal. In order to make the fitting procedure more transparent we have limited ourselves to the following simplified versions of Eq. (3) in the main Manuscript:

$$I_{zzz}^{2\omega} \propto |\chi_{1,zzz}^{(2)} E_{1,z}^2 \sin \theta + \chi_{2,zzz}^{(2)} E_{2,z}^2 \sin \theta|^2 \quad (13)$$

$$I_{xzx}^{2\omega} \propto |\chi_{1,zzz}^{(2)} E_{1,z}^2 \sin \theta + \chi_{2,xzx}^{(2)} E_{2,x} E_{2,z} \cos \theta|^2 \quad (14)$$

$$I_{zxx}^{2\omega} \propto |\chi_{1,zzz}^{(2)} E_{1,z}^2 \sin \theta + \chi_{2,zxx}^{(2)} E_{2,x}^2 \sin \theta|^2, \quad (15)$$

where  $E_1, E_2$  are the calculated electric fields at the bottom and top interfaces, respectively, magnetization-induced  $\chi^{(2,m)}$  components are neglected, and  $\chi_{2,zzz}^{(2)}$ ,  $\chi_{2,xzx}^{(2)}$  and  $\chi_{2,zxx}^{(2)}$  are the complex non-magnetic components of the  $\chi^{(2)}$ -tensor. Additional factors  $\sin \theta$  and  $\cos \theta$  originate from the geometrical projection of the normal ( $z$ ) and tangential ( $x$ ) components of the nonlinear polarisation on the propagation direction of the SHG-beam in the glass prism (see Fig. 4S).

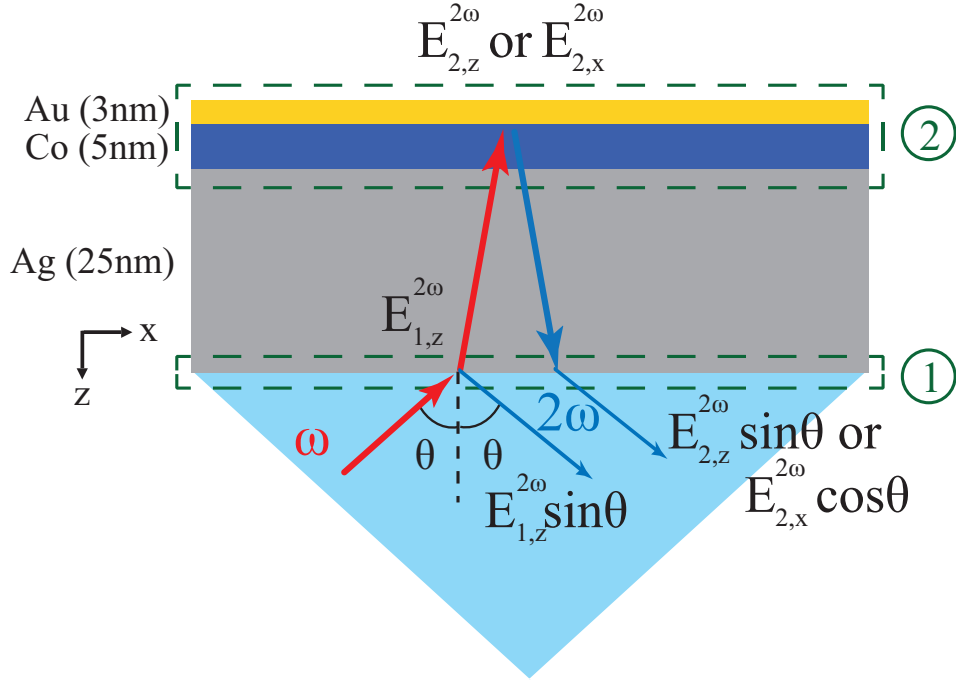


Figure 4S: Geometrical interpretation of SHG in Au/Co/Ag trilayer structure on a glass prism. We assume that SHG occurs at the bottom (1) and top (2) interfaces. SHG electric fields in the glass prism depend on SHG polarization (normal, linearly polarized along the z-direction or tangential, oscillating along the x-direction), which results in an additional geometrical factors  $\sin \theta$  and  $\cos \theta$ .

These equations can be further simplified in order to minimize the number of the fit parameters:

$$I_{zzz}^{2\omega} \propto |E_{1,z}^2 \sin \theta + r_{zzz} E_{2,z}^2 \sin \theta|^2 \quad (16)$$

$$I_{xxx}^{2\omega} \propto |E_{1,z}^2 \sin \theta + r_{xxx} E_{2,x} E_{2,z} \cos \theta|^2 \quad (17)$$

$$I_{zxx}^{2\omega} \propto |E_{1,z}^2 \sin \theta + r_{zxx} E_{2,x}^2 \sin \theta|^2 \quad (18)$$

Without the loss of generality we have used complex coefficients  $r_{zzz}$ ,  $r_{xxx}$  and  $r_{zxx}$  which represent the ratios of the respective  $\chi_{ijk}^{(2)}$ -components to  $\chi_{1,zzz}^{(2)}$  to fit the experimental data. The results of the best fitting shown in Fig. 4S (a) were obtained using  $r_{zzz} = 0.04 \cdot \exp(i1.05\pi)$ ,  $r_{xxx} = 0.19 \cdot \exp(i1.6\pi)$  and  $r_{zxx} = 0.9 \cdot \exp(i0.05\pi)$ , respectively. Three dashed contours illustrate the Lorentzians given by expressions (8,11,12). The nonlinear phase-matching condition shifts the position of SPP-resonance for SHG-generation to larger angles as compared to the linear SPP resonance at  $2\omega$ .

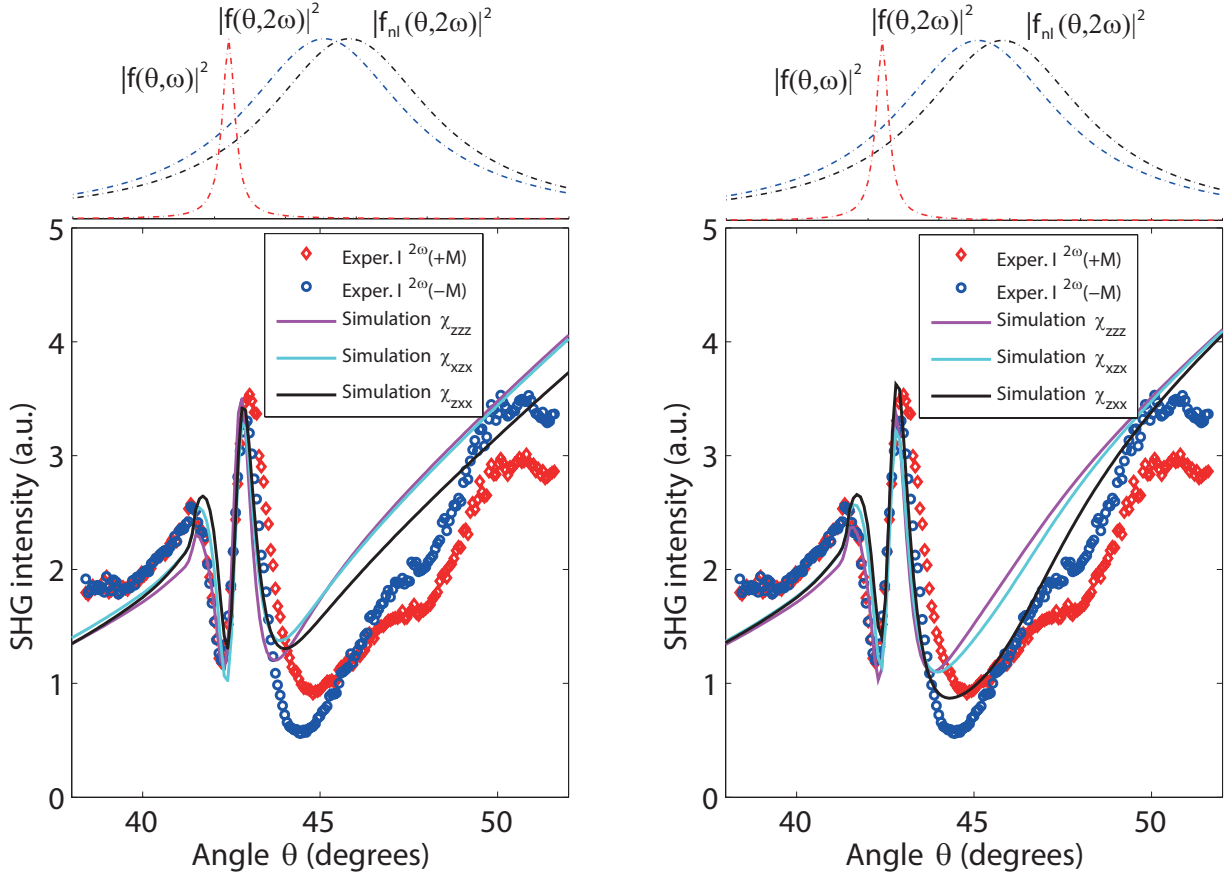


Figure 5S: Angular dependence of SHG intensity for 860 nm optical pump together with best fitting results based on nonresonant  $\chi_{\text{nr}}^{(2)}$  model (a, see Eq. (16-14) and resonant  $\chi_{\text{res}}^{(2)}(\theta)$  model (b, see Eq. (21-19)). Three dashed Lorentzians at the top of the figure aim to illustrate the angular position and width of the SPP-resonances at fundamental and SHG frequencies.

Two main features can be recognized in Figure 5S(a). First, in the vicinity of the fundamental resonance ( $\theta \simeq 42.5^\circ$ ) all three expressions adequately reproduce the experimental data and give almost identical fits. Therefore, our fitting attempts support previously mentioned difficulties and ambiguities [14] in the identification of the dominant  $\chi^{(2)}$  components at arbitrary metal surfaces.

Second, the behavior of our fit curves around  $2\omega$  SPP resonance ( $\theta \simeq 45 - 46^\circ$ ) is notably different from the experiment. This failure to reproduce the experimentally observed SHG intensity minimum stems from the fact that in the above models we have assumed that  $\chi^{(2)}$ -tensor components do not depend on the angle  $\theta$ . This assumption appears to be fundamentally wrong when  $\chi^{(2)}$  contains resonant (SPP-induced) contributions at the SHG frequency  $2\omega$ , thus highlighting one of the most important features in our modeling of the SPP-assisted SHG.

The usual way to take into account SPP-resonance at SHG-frequency  $2\omega$  is based on the representation of  $\chi^{(2)}$ -tensor components as a sum of the non-resonant and resonant contributions [6, 7]:

$$\chi^{(2)} = \chi_{\text{nr}}^{(2)} + \chi_{\text{res}}^{(2)}(\theta). \quad (19)$$

In our case the resonant contribution originates from SPP-excitation at SHG-frequency  $2\omega$ . Whereas the attempts to fit the experimental data shown in Fig. 5S(a) were based on the non-resonant contribution  $\chi^{(2)} \simeq \chi_{\text{nr}}^{(2)}$  (which does not depend on  $\theta$ ), here we focus on the resonant part  $\chi_{\text{res}}^{(2)}(\theta)$ . We assume that the angular dependence of the resonant contribution is as well governed by a Lorentzian shape, which can be obtained from Eq. (9) by linearizing  $\sin \theta$  in the vicinity of  $\theta_{\text{nl}}$ :

$$\chi_{\text{res},ijk}^{(2)}(\theta) = \frac{\Gamma}{\theta - \theta_{\text{nl}} + i\Gamma} r_{ijk}^{(\text{res})} \chi_{1,zzz}^{(2)}. \quad (20)$$

Here  $\Gamma = k''_{\text{spp}}(2\omega)/(k_0(\omega)n(\omega)\cos\theta_{\text{nl}}) = 2.8^\circ$ , and  $\theta_{\text{nl}} = 45.8^\circ$  is given by Eq. (6). The expressions for SHG intensity with resonant contributions  $\chi_{\text{res}}^{(2)}$  thus read:

$$I_{zzz}^{2\omega} \propto |E_{1,z}^2 \sin\theta + r_{zzz}^{(\text{res})} f_{\text{nl}}(\theta) E_{2,z}^2 \sin\theta|^2 \quad (21)$$

$$I_{xzx}^{2\omega} \propto |E_{1,z}^2 \sin\theta + r_{xzx}^{(\text{res})} f_{\text{nl}}(\theta) E_{2,x} E_{2,z} \cos\theta|^2 \quad (22)$$

$$I_{zxx}^{2\omega} \propto |E_{1,z}^2 \sin\theta + r_{zxx}^{(\text{res})} f_{\text{nl}}(\theta) E_{2,x}^2 \sin\theta|^2. \quad (23)$$

The results of the best fitting in Fig. 5S(b) indicate that all three equations with  $r_{zzz}^{(\text{res})} = 0.06 \cdot \exp(i0.3\pi)$ ,  $r_{xzx}^{(\text{res})} = 0.25 \cdot \exp(i0.8\pi)$  and  $r_{zxx}^{(\text{res})} = 1.35 \cdot \exp(i1.25\pi)$ , respectively, provide a better approximation to the experimental data. However, the  $I_{zxx}^{2\omega}$  demonstrates the closest proximity to experimental data thus corroborating our qualitative conclusion that the contributions containing larger local electric fields  $|E_x| \gg |E_z|$  should dominate.

Fitting mSHG and magnetic contrast

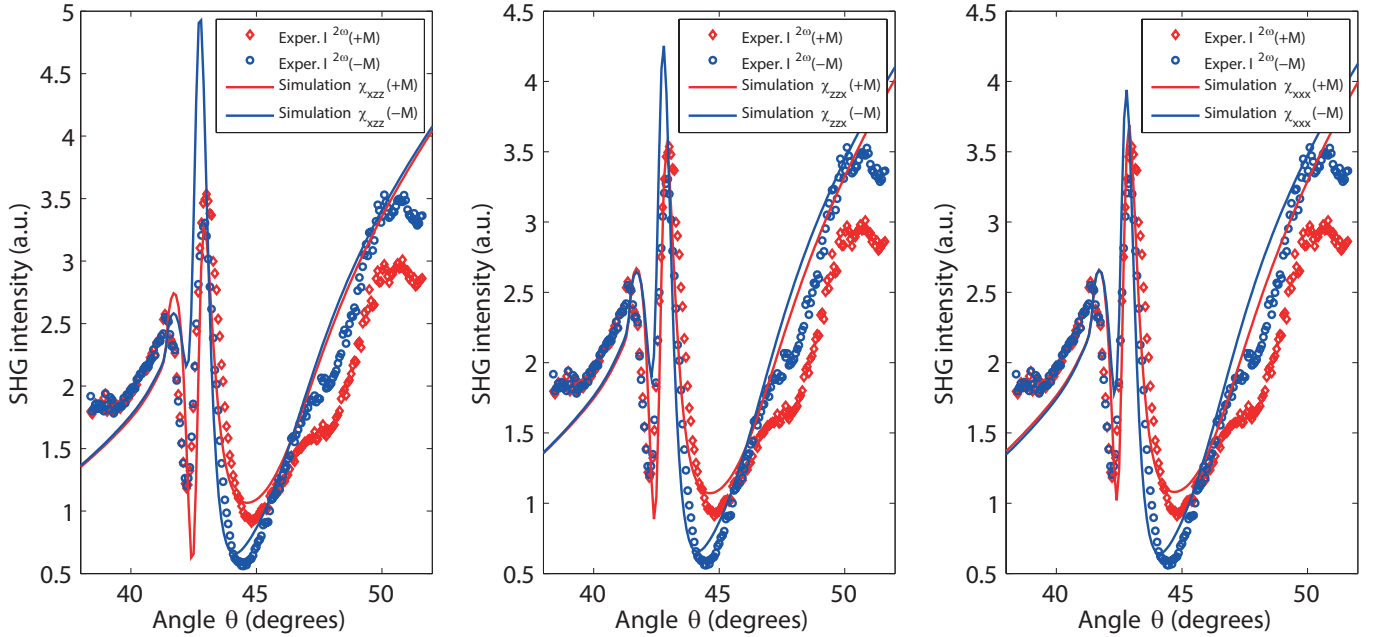


Figure 6S: Angular dependence of SHG intensity for 860 nm optical pump together with best fitting results based on resonant  $\chi_{\text{res}}^{(2)}(\theta)$  model (see Eq. (24-22)) for two opposite orientations of the magnetization  $M$ .

With the results of the two previous sections at hand, we are now ready to fit our experimental SHG intensities and mSHG contrast to the Eq. (3) in the main Manuscript. We note that in the final expression for the SHG intensity we already know the field distributions  $E_{x,z}$ , which account for the SPP resonance at the fundamental frequency  $\omega$ , as well as the resonant contribution of the nonlinear susceptibility  $\chi_{\text{res}}^{(2)}(\theta)$  associated with the SPP resonance at the double frequency  $2\omega$ .

In order to stay in line with systematic fitting procedures we have considered all three magnetic nonlinear susceptibility components  $\chi_{xzz}^{(2,m)}$ ,  $\chi_{zxx}^{(2,m)}$  and  $\chi_{xxx}^{(2,m)}$  [17] leading to the following expressions for the SHG intensities  $I(\pm M)$ :

$$I_{xzz}^{2\omega(m)} \propto |E_{1,z}^2 \sin\theta + r_{xzz}^{(\text{res})} f_{\text{nl}}(\theta) [E_{2,x}^2 \sin\theta \pm r_{xzz}^{(m)} E_{2,z}^2 \cos\theta]|^2 \quad (24)$$

$$I_{zxx}^{2\omega(m)} \propto |E_{1,z}^2 \sin\theta + r_{zxx}^{(\text{res})} f_{\text{nl}}(\theta) [E_{2,x}^2 \sin\theta \pm r_{zxx}^{(m)} E_{2,z} E_{2,x} \sin\theta]|^2 \quad (25)$$

$$I_{xxx}^{2\omega(m)} \propto |E_{1,z}^2 \sin\theta + r_{zxx}^{(\text{res})} f_{\text{nl}}(\theta) [E_{2,x}^2 \sin\theta \pm r_{xxx}^{(m)} E_{2,x}^2 \cos\theta]|^2. \quad (26)$$

Figure 6S shows the final results of our fitting in a direct comparison suggesting that  $I_{xxx}^{2\omega(m)}$  provides the best fitting results, in agreement with our interpretation of dominating terms proportional to  $|E_x(\omega)|^2$ . The angular spectra of the magnetic SHG contrast are presented in Fig. 7S.

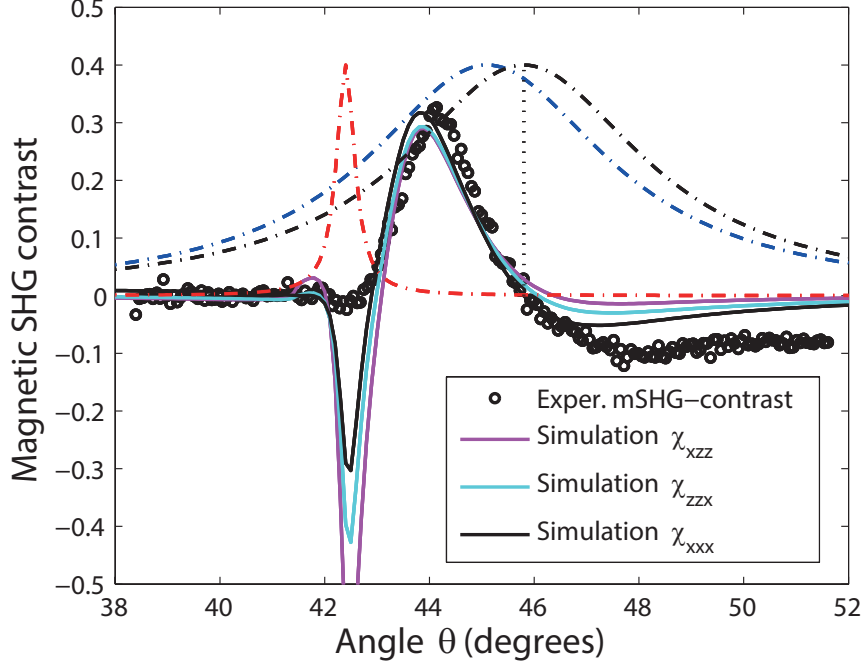


Figure 7S: Angular dependence of mSHG contrast for 860 nm optical pump together with best fitting results based on resonant model with three different magnetic components of  $\chi_{\text{res}}^{(2)}$ -tensor (see Eq. (16-9)). All fits accurately reproduce the behavior of the mSHG contrast in the vicinity of the SHG-resonance and, notably, the sign change at  $\theta_{\text{nl}} = 45.8$  degrees.

The fitting results in Fig. 5S and 6S were obtained with a fixed, previously deduced value  $r_{zxx}^{(\text{res})} = 1.35 \exp(i1.25\pi)$  and using the normalized magnetic components  $r_{ijk}^{(m)} = \chi_{ijk}^{(2,m)} / \chi_{zxx}^{(2)}$  as fit parameters:  $r_{zxx}^{(m)} = 0.02 \cdot \exp(-i0.4\pi)$ ,  $r_{zzx}^{(m)} = 0.07 \cdot \exp(i0.05\pi)$  and  $r_{xxx}^{(m)} = 0.25 \cdot \exp(i0.5\pi)$ . We note that among these values  $r_{xxx}^{(m)}$  is in a good agreement with the results of theoretical calculations for Fe predicting a value  $|r_m| \simeq 0.25$  [18].

The behavior of mSHG contrast in Fig. 7S is accurately reproduced in the vicinity of the SHG-resonance at  $\theta_{\text{nl}} = 45.8^\circ$  but still shows significant deviations at the fundamental SPP-resonance around  $42.5^\circ$ . We attribute these differences to the fact that our simplified model disregards the non-resonant contributions to the  $\chi^{(2)}$ -tensor, the inclusion of which, however, would inevitably stir up troubles related to the multiparameter fitting. Systematic experimental studies of similar multilayer structures with different layer thicknesses should provide more insight about the details of the magnetic SHG and mSHG contrast behaviour at the fundamental SPP-resonance.

- 
- [1] Raether, H. *Surface Plasmons on Smooth and Rough Surfaces and on Gratings*. Springer, 1st Ed., Berlin-Heidelberg (1988).
  - [2] Temnov, V. V. *et al.* Active magneto-plasmonics in hybrid metal-ferromagnet structures. *Nat. Photon.* **4**, 107–111 (2010).
  - [3] Johnson, P. B. & Christy, R. W. Optical Constants of the Noble Metals. *Phys. Rev. B* **6**, 4370–4379 (1972).
  - [4] de Martini, F. & Shen, Y. R. Nonlinear Excitation of Surface Polaritons. *Phys. Rev. Lett.* **36**, 216–219 (1976).
  - [5] Simon, H. J., Benner, R. E. & Rako, J. G. Optical second harmonic generation with surface plasmons in piezoelectric crystals. *Opt. Comm.* **23**, 245–248 (1977).
  - [6] Shen, Y. R. *Principles of Nonlinear Optics*. John Wiley and Sons, Inc., New York (1984).
  - [7] Raschke, M.B., Berweger, S., Atkin, J.M. *Ultrafast and Nonlinear Plasmon Dynamics* in *Plasmonics: Theory and Applications, Challenges and Advances in Computational Chemistry and Physics 15*, T. V. Shahbazyan and M. I. Stockman (eds.), Springer Science+Business Media, Dordrecht (2013).
  - [8] Petukhov, A. V. & Liebsch, A. Surface anisotropy in optical second harmonic generation I. Al(III). *Surf. Sci.* **340**, 195–208 (1995).
  - [9] Guyot-Sionnest, P. & Shen, Y. R. Bulk contribution in surface second-harmonic generation. *Phys. Rev. B* **38**, 7985–7989 (1988).

- [10] Naraoka, R., Okawa, H., Hashimoto, K. & Kajikawa, K. Surface plasmon resonance enhanced second-harmonic generation in kretschmann configuration. *Optics Communications* **248**, 249 – 256 (2005). URL <http://www.sciencedirect.com/science/article/pii/S0030401804012519>.
- [11] Heinz, T.F. *Second-order nonlinear optical effects at surfaces and interfaces* in *Nonlinear Surface Electromagnetic Phenomena*, H.-E. Ponath, and G. I. Stegeman (eds.), Elsevier, Amsterdam (1991).
- [12] Palomba, S. & Novotny, L. Nonlinear excitation of surface plasmon polaritons by four-wave mixing. *Phys. Rev. Lett.* **101**, 056802 (2008). URL <http://link.aps.org/doi/10.1103/PhysRevLett.101.056802>.
- [13] Zheng, W., Hanbicki, A., Jonker, B. T. & Lüpke, G. Control of magnetic contrast with nonlinear magneto-plasmonics. *Sci. Rep.* **4**, 1–5 (2014).
- [14] Simon, H. J., Mitchell, D. E. & Watson, J. G. Optical second-harmonic generation with surface plasmons in silver films. *Phys. Rev. Lett.* **33**, 1531–1534 (1974). URL <http://link.aps.org/doi/10.1103/PhysRevLett.33.1531>.
- [15] Pavlov, V. V. *et al.* Observation of magneto-optical second-harmonic generation with surface plasmon excitation in ultrathin Au/Co/Au films. *Appl. Phys. Lett.* **75**, 190–192 (1999).
- [16] Optical Glass Datasheets, Schott North America, Inc. URL <http://refractiveindex.info>.
- [17] Ru-Pin Pan, Wei, H. D. & Shen, Y. R. Optical second-harmonic generation from magnetized surfaces. *Phys. Rev. B* **39**, 1229–1234 (1989).
- [18] Pustogowa, U. Hübner, W. & Bennemann, K. H. Theory for the nonlinear magneto-optical Kerr effect at ferromagnetic transition-metal surfaces. *Phys. Rev. B* **48**, 8607–8618 (1993).